Available online at www.sciencedirect.com
SCIENCE DIRECT®
ELSEVIER
International Journal of Impact Engineering 32 (2006) 1635–1650
INTERNATIONAL JOURNAL OF IMPACT ENGINEERING
www.elsevier.com/locate/ijimpeng

Spall experiments for the measurement of the tensile strength and fracture energy of concrete at high strain rates

Harald Schuler*, Christoph Mayrhofer, Klaus Thoma

Fraunhofer Institut für Kurzzeitdynamik, Ernst-Mach-Institut, Freiburg, Germany

Received 12 August 2004; received in revised form 27 January 2005; accepted 30 January 2005
Available online 15 April 2005

Abstract

To study the behavior of concrete under dynamic loads, a Hopkinson-Bar was set up and used. Cylindrical concrete specimens were positioned at the end of the incident bar and the spall event was studied. The purpose of this contribution is to explain the measurement of the tensile strength and the specific fracture energy. To determine the tensile strength, the measured free surface velocity at the end of the specimen is used. The method is known from plate impact experiments and was adapted to Hopkinson-Bar experiments. The measurement of the specific fracture energy is more difficult in spall experiments. It cannot be measured directly as it can be done in direct tension tests. A method is proposed where the fracture energy is calculated from the change of the fragment velocities while cracking takes place.

The experimental results of the investigation complete the data of the literature in regard to higher strain rates. In former investigations conducted by Weerheijm (PhD thesis. Delft University of Technology: Delft University Press; 1992), an increase of the specific fracture energy with the strain rate or the crack opening velocity was not seen. The experiments performed within this contribution consider the fracture behavior at higher strain rates. A sharp increase in the specific fracture energy at this strain rates was measured. The following paper describes the method and the experiments to measure the tensile strength and the specific fracture energy in spall experiments.

Keywords: Concrete; Spalling; Hopkinson-Bar; Fracture energy; Tensile strength; DIF

*Corresponding author.
E-mail address: harald.schuler@emi.fhg.de (H. Schuler).

0734-743X/$ - see front matter © 2005 Elsevier Ltd. All rights reserved.
doi:10.1016/j.ijimpeng.2005.01.010

Notation

A_{frac}, A_n, A fracture surface, cross section at the notch, cross section
C_0 wave propagation velocity in a slender bar (1D-stress)
DIF, DIF_G Dynamic intensification factor: strength, specific fracture energy
E_{qs}, E_{dyn} quasi-static, dynamic Young's modulus
G_{fqs}, $G_{fdyn} = Gf_{dyn}/A_{frac}$ quasi-static, dynamic specific fracture energy
Gf_{dyn} dynamic fracture energy
I impulse
v particle velocity
δ, $\dot{\delta}$ crack opening, crack opening velocity
$\dot{\varepsilon}$ strain rate
ρ density
σ stress
σ_{fqs}, σ_{fdyn} quasi-static, dynamic tensile strength
σ_i, σ_t, σ_r incident, transmitted and reflected signal

1. Introduction

Material data are elementary when simulating concrete under high loading rates (Riedel [22], Schuler et al. [23], Sluys [24]). Models of concrete for static applications have to be extended by dynamic material properties. The strength of concrete for tensile and compressive loading increases with the loading rate. Several investigations have been performed to study this effect. Especially in the case of tensile loading, a sharp increase in the strength is measured at high loading rates. Direct tension tests with a Split–Hopkinson-Bar are suitable to study the tensile strength for strain rates between 10^{-1} and 10^{1} 1/s. Extensive investigations have been performed by Weerheijm [1], Zielinski [2], Ross [3], Zheng [4] and Birkimer et al. [13]. Higher strain rates up to 10^{2} 1/s can be achieved by spall experiments. In spall experiments, the tensile stresses arise from the reflection of a compression wave at the free end of the specimen. Mac Vay [5] conducted spall tests on concrete slabs by lighting an explosive at a certain distance. Via a geometric relation he determined the strength in the spall plane. Besides the blasting of concrete slabs most spall experiments were performed with a Hopkinson-Bar. Klepaczko and Brara [6] performed a large number of spall experiments investigating wet and dry specimens. In the case of wet specimens, a strength increase up to a factor of 13 compared to the static strength was observed. In the case of dry specimens they measured a strength increase up to a factor of 8.5. A valuable review of several tension experiments especially in the strain rate range higher than 10^{0} 1/s is given by Malvar and Ross [7].

Many experiments have been performed for the measurement of the tensile strength over a wide range of strain rates, whereas only a few data are available of the specific fracture energy. The specific fracture energy is needed to model the softening behavior of brittle materials. Material models including this parameter have the ability of objective solutions regarding the change of the mesh size. There is a need of data of the specific fracture energy at higher strain rates. Weerheijm

[1] measured in direct tension tests with a Hopkinson-Bar the complete stress-crack opening relation. He could specify the fracture energy at strain rates between 10^{-1} and 10^{0} 1/s. In this contribution, the focus is to measure the specific fracture energy at strain rates between 10^{1} and 10^{2} 1/s. This can be reached by spall experiments.

2. Loading principle and applied method for the measurement of tensile strength and specific fracture energy

A Split-Hopkinson-Bar device was modified to investigate the tensile behavior of concrete under high loading rates. The setup consists of a projectile, an incident bar and the specimen. The transmitter bar was removed (cf. Fig. 1). In order to measure the waves, strain gages were applied at the incident bar. The free surface velocity at the end of the specimen was determined via integration of the acceleration signal. Concrete specimens with a length of 250 mm and a diameter of 74.2 mm were investigated. The uniaxial compressive strength of the used concrete was not measured but was approximately 35 MPa. The maximum aggregate size was 8 mm.

Fig. 2 illustrates the principle of the loading in a spall test. After the impact of the projectile, an incident wave σ_i propagates in the bar. One part is transmitted into the specimen σ_t and another one is reflected at the interface between bar and specimen σ_r. The transmitted compression wave is reflected at the free end and becomes a tensile wave. This leads to fracture in the spall plane.

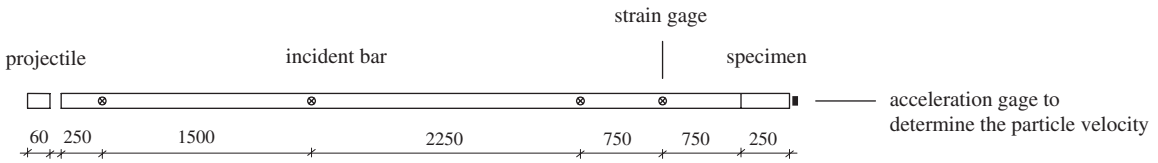

Fig. 1. Hopkinson-Bar (mm) with strain gages and an acceleration gage at the free end of the specimen.

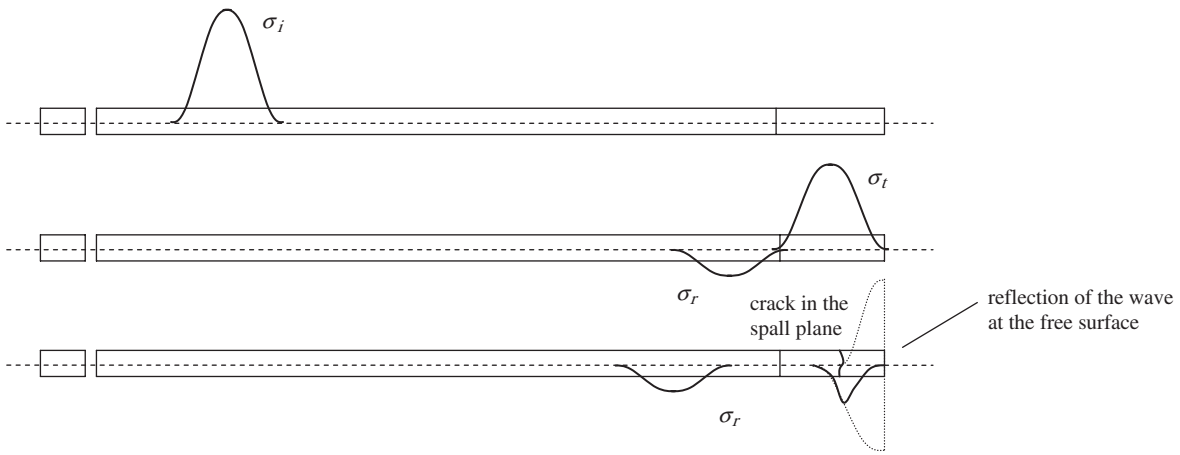

Fig. 2. Spall experiment to determine dynamic fracture parameter with a modified Split-Hopkinson-Bar device.

Spall experiments are restricted to brittle materials that have a much higher compressive strength than tensile strength. Otherwise the specimen would be predamaged through the compression wave.

To measure Young's modulus, tensile strength and fracture energy, the following approach was used. The starting point was the measured strain at the last strain gage on the incident bar (cf. Fig. 1).

2.1. Measurement of the wave velocity and the dynamic Young's modulus E_{dyn}

The first step was the shifting of the wave to the end of the incident bar. The wave shifting includes a dispersion correction that is described in Zheng [4], Gong et al. [8] and Bancroft [11] for instance. Eq. (1) presents the dispersion corrected signal at the end of the incident bar. The different wave velocities of the different wavelengths were corrected by the phase shifts ϕ_{dn}.

$$\varepsilon_{\mathrm{alu}}(t) = \frac{A_0}{2} + \sum_{n=1}^{\infty} D_n \cos(n\omega_0 t - (\phi + \phi_{dn})). \tag{1}$$

The wave velocity C_0 and the dynamic Young's modulus E_{dyn} were calculated, with the signal at the beginning of the specimen (calculated from Eq. (1)) and the measured free surface velocity at the end of the specimen. The time Δt that the wave needs to propagate from the beginning to the end of the specimen is read off the diagram in Fig. 3.

$$C_0 = \frac{L}{\Delta t} \Rightarrow E_{\mathrm{dyn}} = \rho C_0^2. \tag{2}$$

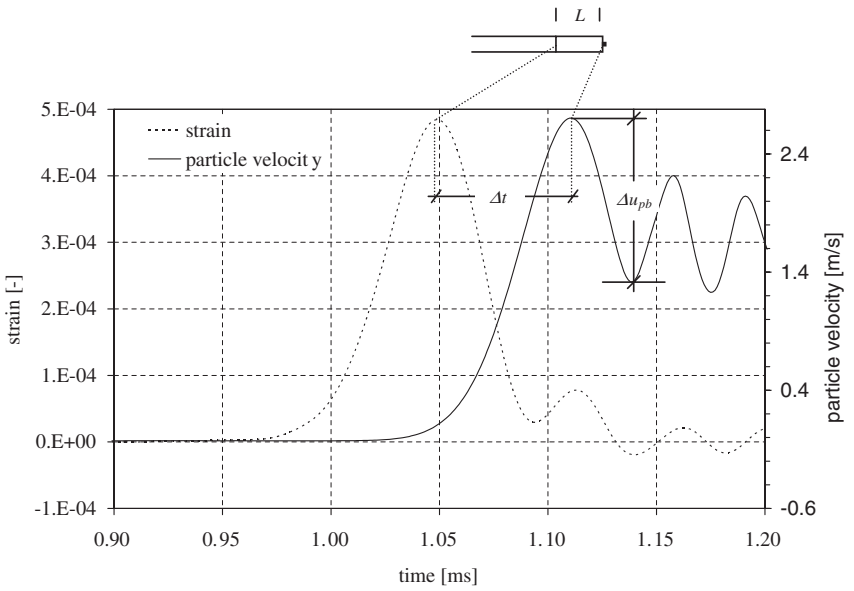

Fig. 3. Strain at the end of the incident bar (beginning of the specimen) and particle velocity at the end of the specimen; time Δt that the wave needs to propagate from the beginning to the end of the specimen.

2.2. Measurement of the dynamic tensile strength σ_{fdyn}

The dynamic tensile strength can be measured directly from the free surface velocity. Therefore the "pull-back" velocity Δu_{pb} was determined from the velocity measurement. In Fig. 3, Δu_{pb} is marked. With the density ρ and the wave propagation velocity C_0 of concrete, the tensile strength could be calculated. It should be mentioned that Eq. (3) is usually used in plate impact experiments with the longitudinal wave velocity C_l for 1D-strain conditions (Arnold [10], Zukas [26]). Using C_0 instead of C_l yields the tensile strength under 1D-stress conditions:

$$\sigma_{fdyn} = \tfrac{1}{2}\rho C_0 \Delta u_{pb}. \tag{3}$$

2.3. Measurement of the dynamic fracture energy Gf_{dyn}

In spall experiments, it is not possible to measure stress over strain or crack opening as it can be done in quasi-static tension tests. For this reason, the fracture energy was calculated from the reduction of the fragment velocities. Two points of time were considered while crack opening takes place: $t1$, time where crack initiation starts; $t2$, time where the crack is completely opened.

The dissipated energy between the time $t1$ and the time $t2$ is the fracture energy. The following method specifies how the fracture energy was determined from the reduction of the fragment velocities. A typical fracture image is shown in Fig. 4.

To obtain the velocity at the time $t1$ where crack initiation starts, the stress and velocity distribution in the specimen was calculated analytically. In the case of stress, an imaginary mirrored wave was subtracted from the transmitted wave. In the case of velocity the signals were added. Fig. 5 and Eqs. (4) and (5) specify the superposition of the two waves in order to obtain the stress and the velocity as a function of the position x and the time t:

$$\sigma(x,t) = \sigma\left(t - \frac{x}{C_0}\right) - \sigma\left(t + \frac{x - 2x_{end}}{C_0}\right), \tag{4}$$

$$v(x,t) = \frac{C}{E}\sigma\left(t - \frac{x}{C_0}\right) + \frac{C}{E}\sigma\left(t + \frac{x - 2x_{end}}{C_0}\right), \tag{5}$$

where $\sigma(t)$ is the transmitted stress wave into the specimen that was calculated from Eq. (1). The solution of Eqs. (4) and (5) is shown in Fig. 6 for different points of times with a resolution of 5 μs. The period where the tensile wave occurs is plotted. The bold lines are the lines where the tensile stress reaches the tensile strength which is already measured in Section 2.2. At this point of time,

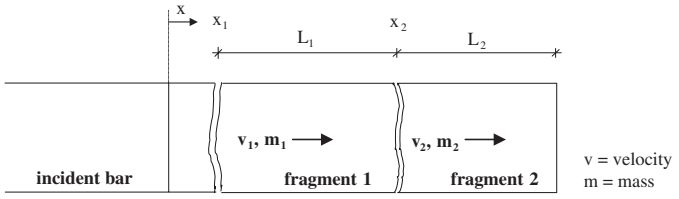

Fig. 4. Typical fracture image with two fragments.

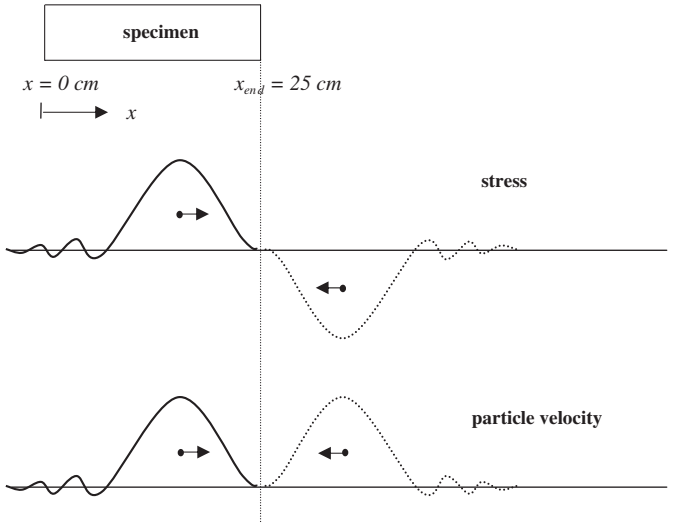

Fig. 5. Reflection of the wave at the free surface: superposition with a fictive contrarily propagating wave.

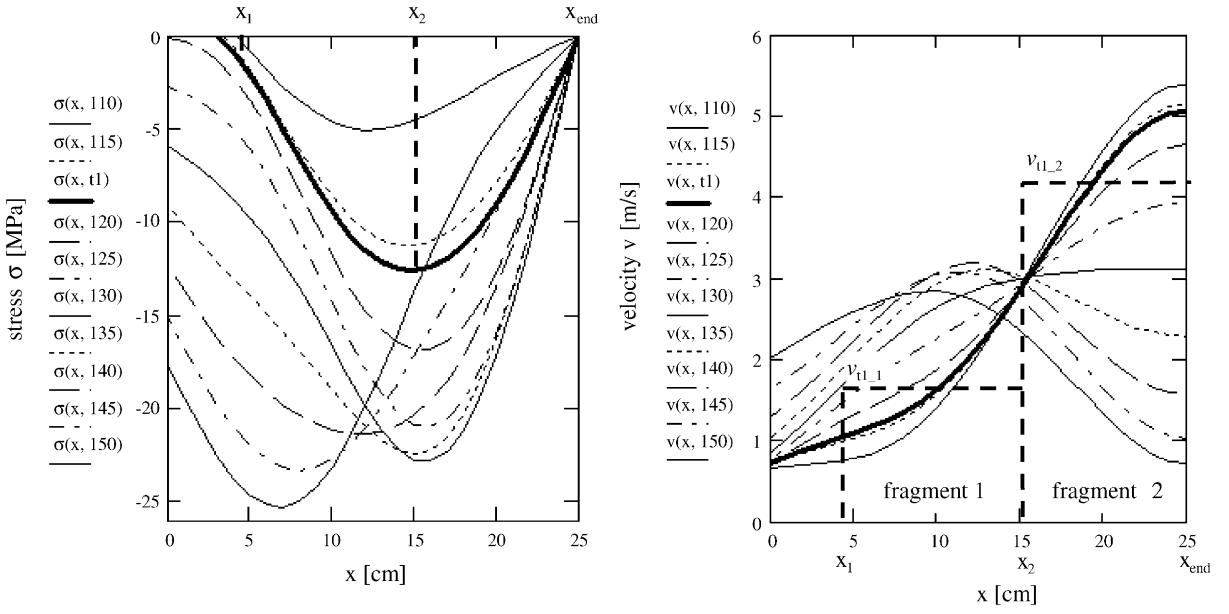

Fig. 6. Stress and particle velocity distribution in the 25 cm long specimen printed every 5 μs, while the tensile wave comes up.

the fracture process started ($t1$) and the mean velocities v_{t1_1} and v_{t1_2} of fragments 1 and 2 could be read from the diagram on the right in Fig. 6. The velocities of the fragments after the fracture process is finished ($t2$), v_{t2_1} and v_{t2_2}, were measured using a high-speed camera.

The fracture energy is the integral of the force F over the crack opening δ and can be rewritten as a function of the impulse change $\mathrm{d}I$ and the crack opening velocity $\dot{\delta}$:

$$Gf = \int F \,\mathrm{d}\delta = \int \frac{\mathrm{d}I}{\mathrm{d}t}\dot{\delta}\,\mathrm{d}t. \tag{6}$$

Over the whole fracture process the impulse transfer ΔI from fragment 1 to fragment 2 and the corresponding mean crack opening velocity $\dot{\delta}$ are

$$\Delta I = I_{1\_2} = (v_{t1\_2} - v_{t2\_2})m_2, \tag{7}$$

$$\dot{\delta} = \dot{\delta}_{1\_2} = \frac{v_{t2\_2} + v_{t1\_2}}{2} - \frac{v_{t2\_1} + v_{t1\_1}}{2}, \tag{8}$$

where m_2 is the mass of the second fragment.

With these values the fracture energy is simplified:

$$Gf = \Delta I\dot{\delta}. \tag{9}$$

2.4. Measurement of the fracture surface

The fracture energy has to be divided through the fracture surface in the spall plane to obtain the specific fracture energy, which is used as an input parameter in the numerical simulation. In the case of notched specimens, the fracture surface is equal to the cross section at the notch. In the case of specimens without a notch the measurement of the fracture surface is more difficult. An estimate of the fracture surface can be reached by a microscopic inspection along the circumference. Fig. 7 shows an image formed from eight pictures around the specimen surface. The cracks in the neighborhood of the spall plane are signed with a black pen and the ratio between the accumulated crack length and the circumferential length is built. This ratio is simplified equal to the ratio between the fracture surface and the cross-sectional area A_{frac}/A. The ratios A_{frac}/A are listed in Tables 3 and 6.

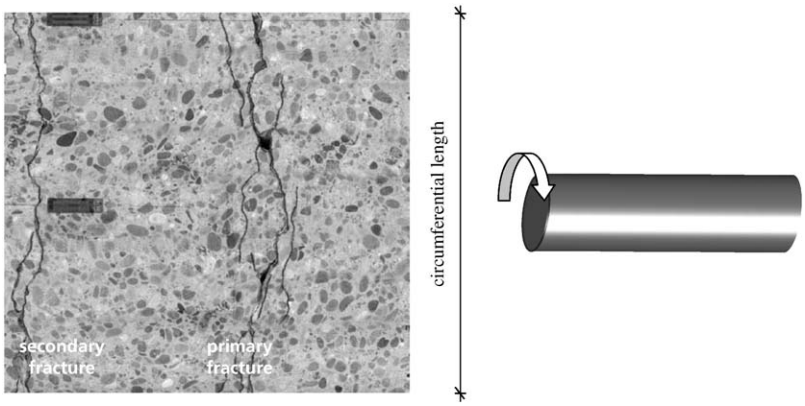

Fig. 7. Cracks along the circumference measured with a microscope (minimal crack width approx. 50 μm).

3. Experiments

The investigation contains unnotched specimens that were glued to the incident bar and notched specimens that were laid in contact to the incident bar. The scope of investigation is described in Table 1.

With different projectile velocities the strain rate could be varied in the specimen in a small range. The advantage of unnotched specimens (load stage 1–3) is that a uniaxial stress state predominates in the specimen. In the case of an applied notch, the stress state is not uniaxial. But for a notched specimen, the fracture surface is clearly defined as the reduced cross section. So both notched and unnotched specimens have advantages and disadvantages. Hence both approaches were followed.

3.1. Load stage 1

Fig. 8 presents the fractured specimens apart and put together. One breach occurred at the primary fracture zone.

Table 1
Scope of investigation

Load stage	Number of specimen	Projectile velocity (m/s)	$\dot{\varepsilon}$ (1/s)
1	4	4.1	33
2	4	7.6	68
3	4	11.1	80
Notched	4	3.4	31

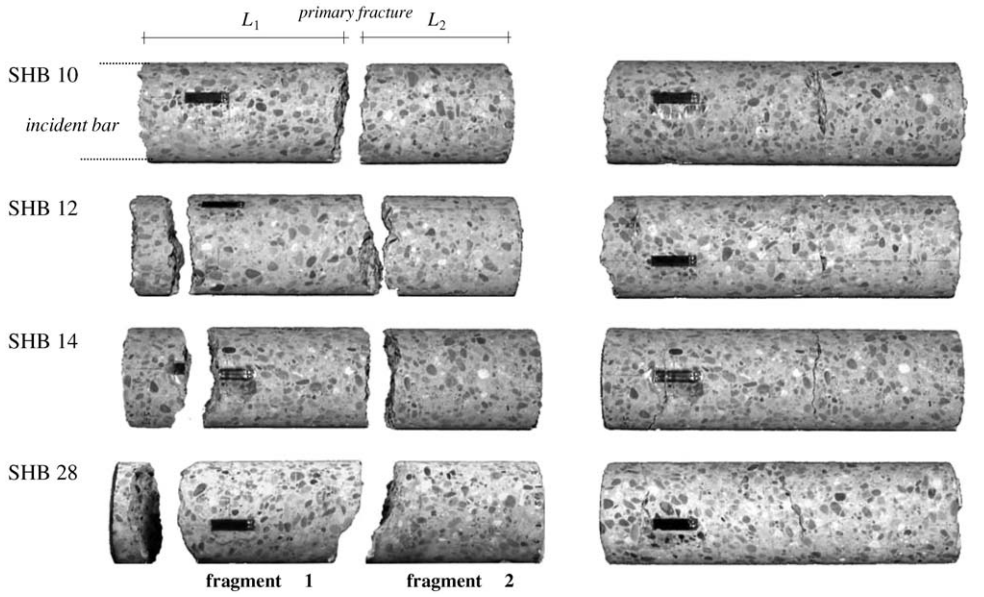

Fig. 8. Fragments lying apart (left) and put together (right).

Table 2
Length (weight) of the fragments and their velocity at times $t1$ and $t2$

Specimen	l_1 (mm) (m_1) (kg)	l_2 (mm) (m_1) (kg)	v_{t1_1} (m/s)	v_{t1_2} (m/s)	v_{t2_1} (m/s)	v_{t2_2} (m/s)
SHB 10	142 (1.43)	103 (1.04)	1.26	4.16	1.00	3.40
SHB 12	131 (1.32)	90 (0.91)	1.73	4.54	1.38	2.63
SHB 14	110 (1.11)	102 (1.03)	1.66	4.20	0.68	3.03
SHB 28	109 (1.10)	112 (1.13)	1.87	3.61	1.02	1.82

Table 3
Measured material properties evaluated as described in Section 2

Specimen	E_{dyn} (GPa)	σ_{fdyn} (MPa)	Gf_{dyn} (J)	A_{frac}/A (–)	Gf_{dyn}/A_{frac} (J/m^2)	$\dot{\varepsilon}$ (1/s)	$\dot{\delta}$ (m/s)
SHB 10	38.6	13.2	2.09	2.76	175.3	37.1	2.65
SHB 12	41.4	14.3	3.52	2.65	307.1	37.9	2.03
SHB 14	39.9	12.5	2.94	1.83	371.3	33.6	2.45
SHB 28	40.4	11.5	2.57	1.98	299.9	23.5	1.27
Average	40.1 ± 1.0	12.9 ± 1.0	2.78	2.31	288.5 ± 71.0	33.0	2.10

Fig. 6 and Table 2 show that the primary fracture occurred always in a distance of 90–112 mm to the right end of the specimen. The secondary fracture appeared near the glued joint to the incident bar.

The mechanical properties were determined as described in Section 2 and are summarized in Table 3. The strain rate $\dot{\varepsilon}$ was calculated from the rise time of the tensile wave.

3.2. Load stage 2

Specimens loaded with the second load stage showed at least one additional fragment at the primary fracture zone. The mean length and the mass of the fragments are listed in Table 4. In Table 5, the corresponding velocity at the time when the crack initiation starts, $t1$, and when the crack is completely opened, $t2$, are listed.

As already mentioned, at least one additional fragment occurred in load stage 2. This had to be taken into account by the calculation of the impulse transfer (cf. Eq. (7)). In the case of one additional fragment, the impulse transfer had to be considered from fragment 3 to fragment 2, I_{2_3}, and from fragment 2 to fragment 1, I_{1_2} (cf. Fig. 9). In this case, the impulse transfer had to be calculated by the following equations:

$$I_{2\_3} = I_{t1\_3} - I_{t2\_3},$$
$$I_{1\_2} = I_{t1\_2} - I_{t2\_2} + I_{2\_3}. \tag{10}$$

For both impulse transfers I_{2_3} and I_{1_2}, the fracture energies were calculated and added. The crack opening velocities $\dot{\delta}_{2\_3}$ and $\dot{\delta}_{1\_2}$ were calculated between fragments 2 and 3 and fragments 1 and 2, and the mean value $\dot{\delta}$ was built. In Table 6, the measured material properties are summarized.

Table 4
Length and weight of the fragments

Specimen	L_1 (mm)	L_2 (mm)	L_3 (mm)	L_4 (mm)	m_1 (kg)	m_2 (kg)	m_3 (kg)	m_4 (kg)
SHB 16	135	12	94	—	1.36	0.12	0.95	—
SHB 17	124	38	76	—	1.25	0.38	0.76	—
SHB 25	109	25	45	68	1.10	0.26	0.46	0.68
SHB 26	133	33	79	—	1.35	0.33	0.81	—

Table 5
Velocity of the fragments at times $t1$ and $t2$

Specimen	v_{t1_1} (m/s)	v_{t1_2} (m/s)	v_{t1_3} (m/s)	v_{t1_4} (m/s)	v_{t2_1} (m/s)	v_{t2_2} (m/s)	v_{t2_3} (m/s)	v_{t2_4} (m/s)
SHB 16	—	—	—	—	—	—	—	—
SHB 17	2.27	5.06	8.07	—	2.93	3.53	7.13	—
SHB 25	2.32	3.66	5.48	9.03	1.90	2.25	5.60	7.65
SHB 26	1.78	5.17	8.86	—	2.68	3.96	7.4	—

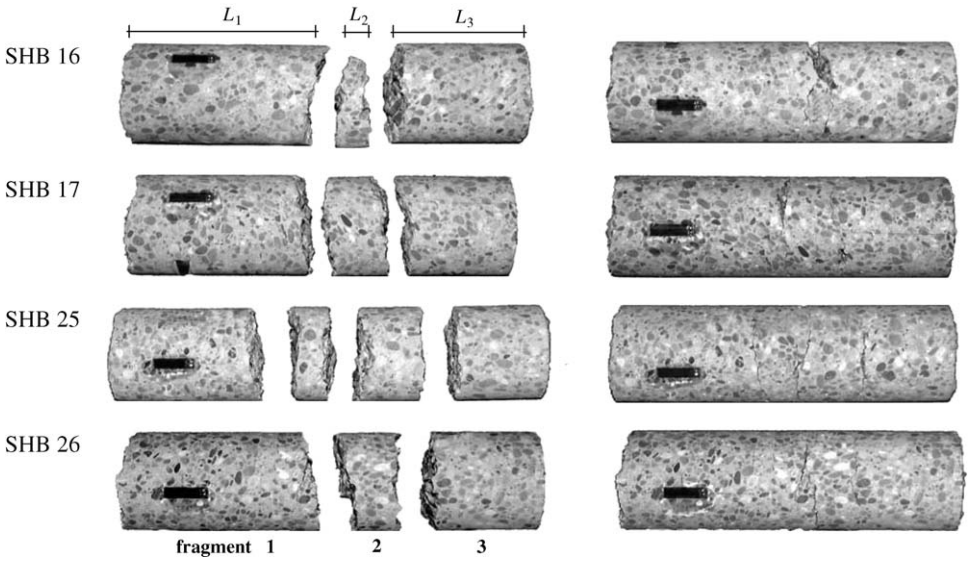

Fig. 9. Fragments lying apart (left) and put together (right).

Table 6
Measured material properties evaluated as described in Section 2

Specimen	E_{dyn} (GPa)	σ_{fdyn} (MPa)	Gf_{dyn} (J)	A_{frac}/A (–)	Gf_{dyn}/A_{frac} (J/m^2)	$\dot{\varepsilon}$ (1/s)	$\dot{\delta}$ (m/s)
SHB 17	37.7	16.0	4.57	3.97	266.8	59.1	2.50
SHB 25	39.3	18.7	6.01	4.97	279.9	72.1	2.08
SHB 26	40.0	17.1	7.83	3.97	456.7	72.5	2.95
Average	38.7 ± 1.0	16.2 ± 2.0	6.14	4.30	334.5 ± 86.6	67.8	2.51

3.3. Load stage 3

In the third load stage, multiple fragments appeared at the primary fracture zone, so that it was difficult or inaccurate to measure the fracture energy. Hence in load stage 3 only the Young's modulus and the tensile strength were measured. The fractured specimens are shown in Fig. 10 and can be compared with the results of load stages 1 and 2.

In Table 7 the measured material properties are given.

3.4. Notched specimen

Notched specimens have the advantage that the fracture surface is defined as the cross section at the position of the notch A_n. To calculate the tensile strength from the "pull-back" velocity Δu_{pb}, the ratio A/A_n has to be added to Eq. (3):

$$\sigma_{fdyn} = \frac{A}{2A_n}\rho C_0 \Delta u_{pb}. \tag{11}$$

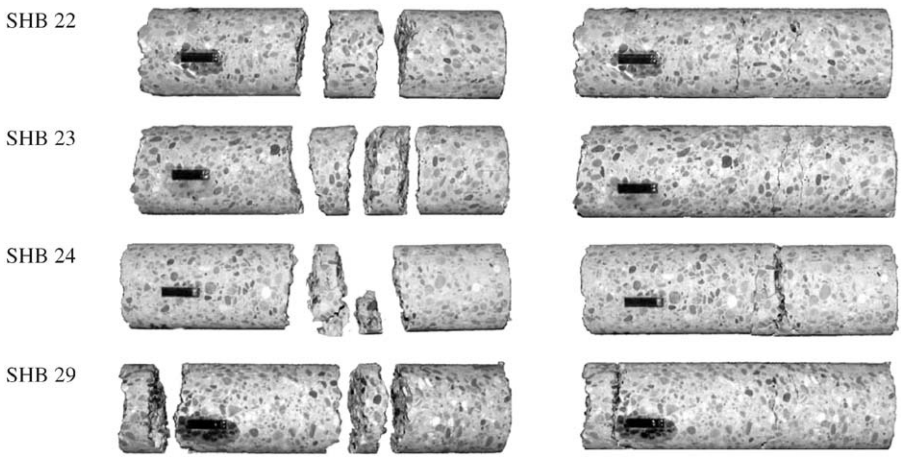

Fig. 10. Fragments lying apart (left) and put together (right).

Table 7
Measured material properties evaluated as described in Section 2

Specimen	E_{dyn} (GPa)	σ_{fdyn} (MPa)	$\dot{\varepsilon}$ (1/s)
SHB 22	40.8	19.1	93.6
SHB 23	39.5	18.0	77.8
SHB 24	39.7	—	—
SHB 29	39.7	16.8	67.2
Average	39.9 ± 0.5	18.0 ± 0.9	79.5

Table 8
Velocity of the fragments at times $t1$ and $t2$

Specimen	v_{t1_1} (m/s)	v_{t1_2} (m/s)	v_{t2_1} (m/s)	v_{t2_2} (m/s)
SHB 60	1.02	3.50	1.64	2.94
SHB 62	1.02	3.24	1.68	2.16
SHB 63	1.11	3.48	1.59	2.62
SHB 64	1.13	3.06	1.86	2.26

Table 9
Measured material properties evaluated as described in Section 2

Specimen	E_{dyn} (GPa)	σ_{fdyn} (MPa)	Gf_{dyn}/A_n (J/m^2)	$\dot{\varepsilon}$ (1/s)	$\dot{\delta}$ (m/s)
SHB 60	37.6	14.6	325.4	32.4	1.89
SHB 62	37.3	13.6	451.4	29.3	1.35
SHB 63	36.5	17.6	455.7	33.5	1.70
SHB 64	37.7	16.4	289.2	27.7	1.17
Average	37.3 ± 0.5	15.6 ± 1.6	380.4 ± 74.3	30.7	1.53

In this case the specimens were laid in contact to the incident bar with a thin layer of plaster in order to clear the unevenness of the specimen. The notch with a depth of 5 mm was positioned at the place where the primary fracture occurred in the former experiments. This was in a distance of about 100 mm from the free end of the specimen. The mass of fragment 1 was approximately 1.5 kg and of fragment 2 was about 1.0 kg. The velocity of the fragments at the beginning of the breach ($t1$) and when the crack was totally opened ($t2$) are given in Table 8.

The fracture energy was calculated in the same way as for the unnotched specimens. The results are listed in Table 9.

4. Experimental results in comparison to literature data

Young's Modulus E_{dyn}: The dynamic Young's modulus E_{dyn} which is calculated from the wave propagation velocity is nearly constant in load stages 1 and 2. The quasi-static Young's modulus is measured in a uniaxial compression test. The mean value for quasi-static loading $E_{qs} = 38.9$ GPa is nearly equal to the mean value of dynamic loading $E_{dyn} = 39.6$ GPa. Thus we conclude that there is no significant dependence on the strain rate. The Young's modulus measured with notched specimens is less reliable because of the stress state around the notch.

Tensile strength σ_{fdyn}: At strain rates between 10^1 and 10^2 1/s, an increase by a factor of $\sigma_{fdyn}/\sigma_{fqs} = 4$–$5.5$ was measured. In Fig. 11, the results are plotted together with literature data. To obtain the quasi-static tensile strength, Brazilian tests were performed. The tensile strength σ_{fqs} is established to 90% of the splitting tensile strength measured in the Brazilian tests. The mean value of the quasi-static tensile strength was $\sigma_{fqs} = 3.24$ MPa.

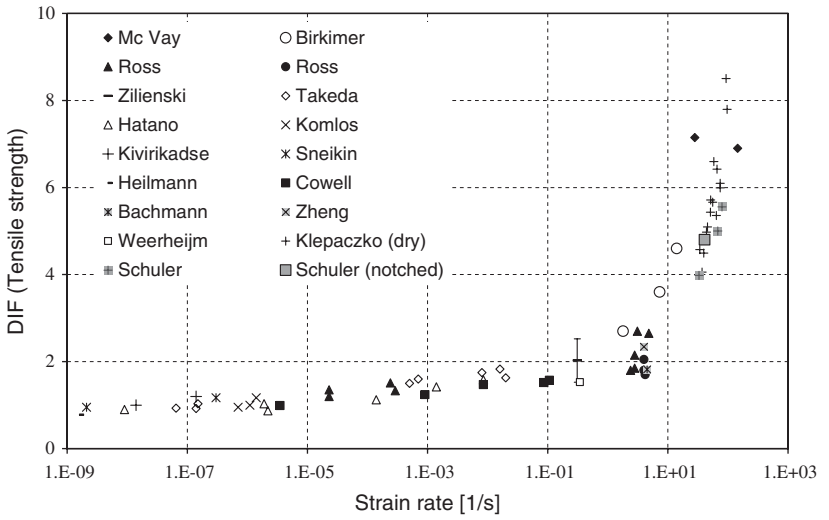

Fig. 11. Dynamic intensification factor DIF $= \sigma_{\mathrm{fdyn}}/\sigma_{\mathrm{fqs}}$ for the tensile strength.

Specific fracture energy G_{fdyn}: The measured fracture energies and the corresponding fracture surfaces are illustrated in Fig. 12. The diagram shows that with increasing strain rate, which is also an increase in the load, the fracture energy increases. However, the fracture surface area also increases, which means that in the range of strain rates between 10^1 and 10^2 1/s, the specific fracture energy is nearly constant (cf. Tables 3 and 6). The behavior that at higher loads more fracture surfaces emerge can also be seen in the differences between the fracture images in Figs. 8–10.

The static reference value for the specific fracture energy was measured in three-point-bending-tests on notched beams as proposed by RILEM [9]. The measured static specific fracture energy was $G_{\mathrm{fqs}} = 125.0\,\mathrm{J/m^2}$. In Fig. 13, the specific fracture energy measured by Weerheijm [1] in direct tension tests is plotted. In his Hopkinson-Bar experiments, he reached a strain rate of approximately 0.3 1/s. Up to this loading velocity, an increase in the specific fracture energy was not observed. At higher loading velocities, achieved by spall experiments, the increase was of a factor of two to three compared to quasi-static experiments. The performed experiments are plotted in Fig. 13.

A proposal for the dependence of the specific fracture energy from the crack opening velocity $\dot{\delta}$ is subsequently given. This corresponds to the dashed line in Fig. 13.

$$\mathrm{DIF}_G = \frac{G_{\mathrm{fdyn}}}{G_{\mathrm{fqs}}} = 1, \quad \dot{\delta} \leqslant 0.33\ \mathrm{m/s},$$

$$\mathrm{DIF}_G = \frac{G_{\mathrm{fdyn}}}{G_{\mathrm{fqs}}} = A\dot{\delta}^B, \quad \dot{\delta} > A^{-1/B} = 0.33\ \mathrm{m/s}, \tag{12}$$

with $A = 1.74$ and $B = 0.5$, $\dot{\delta}$ in m/s.

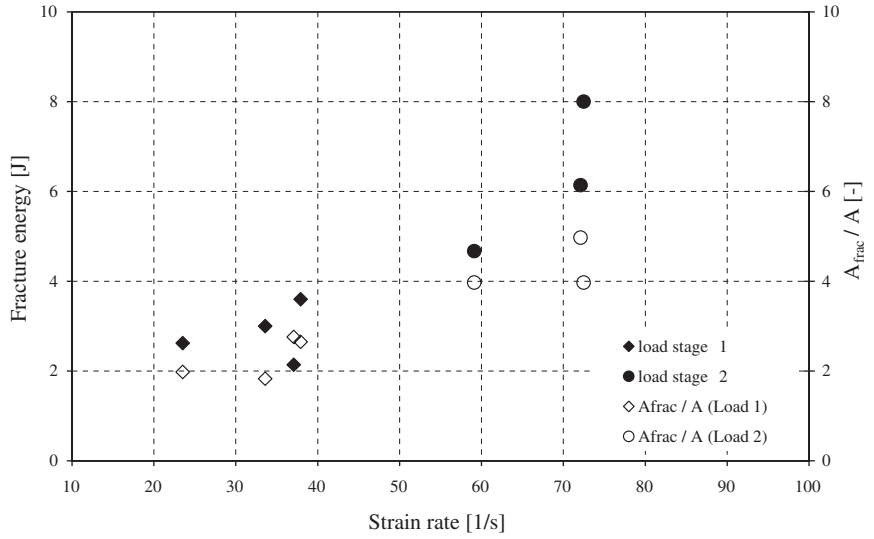

Fig. 12. Fracture energy Gf_{dyn} and the according relative fracture surface A_{frac}/A taken from Tables 3 and 6.

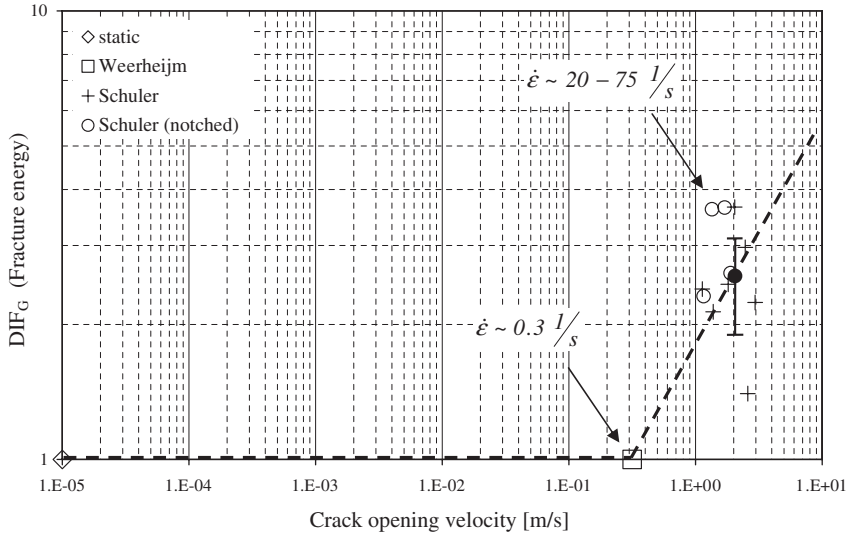

Fig. 13. Dynamic intensification factor $\mathrm{DIF}_G = G_{\mathrm{fdyn}}/G_{\mathrm{fqs}}$ for the specific fracture energy: literature data and measured data from Tables 3, 6 and 9.

The approach can be used in material models which uses the specific fracture energy to describe the tensile softening. According to Tables 3, 6 and 9, it is also possible to specify the specific fracture energy as a function of the strain rate.

5. Conclusion

The purpose of the experimental study was the measurement of the tensile strength and in particular the specific fracture energy of concrete. It is established that a sharp increase in the tensile strength exists at strain rates higher than 10 1/s. The question was if such an increase exists also for the specific fracture energy. To date, there was no investigation concerning the fracture energy at spall loading. At lower loading velocities no increase of the specific fracture energy was observed.

With a Hopkinson-Bar the spall behavior was investigated. To measure the tensile strength the free surface velocity was used as is done for plate impact experiments. The results confirm experiments given in the literature (e.g. [6]). The fracture energy cannot be measured directly. This paper shows a method that is appropriate to determine the specific fracture energy from the change of the fragment velocities while cracking emerges. Several spall experiments on plane and notched specimens have been performed. A dynamic intensification factor for fracture energy DIF_G between 2 and 3 was measured.

The specific fracture energy is a material parameter that is needed for numerical simulations. The damage of concrete under explosive loading, the break-up phenomenon and fragment velocities are all highly influenced by the fracture energy.

References

[1] Weerheijm J. Concrete under impact tensile loading and lateral compression. PhD thesis. Delft University of Technology: Delft University Press; 1992.
[2] Zielinski AJ. Fracture of concrete and mortar under uniaxial impact tensile loading. PhD thesis. Delft University of Technology: Delft University Press; 1982.
[3] Ross A. Split–Hopkinson pressure bar tests. 1989.
[4] Zheng S. Beton bei variierender Dehngeschwindigkeit untersucht mit einer neuen modifizierten Split–Hopkinson-Bar-Technik. PhD thesis, vol. 27. University Karlsruhe: Schriftenreihe des Instituts für Massivbau und Baustofftechnologie; 1996.
[5] McVay MK. Spall damage of concrete structures. Technical Report No. SL-88-22, US Army Engineer Waterways Experiment Station, Vicksburg, June 1988.
[6] Klepaczko JR, Brara A. An experimental method for dynamic tensile testing of concrete by spalling. Int J Impact Eng 2001;25:387–409.
[7] Malvar JM, Ross CA. Review of strain rate effects for concrete in tension. ACI Mater J 1998;95(6):735–9.
[8] Gong JC, Malvern LE, Jenkins DA. Dispersion investigation in the Split Hopkinson pressure bar. J Eng Mater Technol 1990;112:309–14.
[9] RILEM 1985-TC 50-FMC. Determination of the fracture energy of mortar and concrete by means of three-point bend tests on notched beams. RILEM Recommend Mater Struct 18(106).
[10] Arnold W. Dynamisches Werkstoffverhalten von Armco-Eisen bei Stoßwellenbelastung. PhD thesis, vol. 5. Technical University Muenchen: VDI-Forschungsberichte; 1992. p. 247.
[11] Bancroft D. The velocity of longitudinal waves in cylindrical bars. Phys Rev 1941;59:588–93.
[13] Birkimer DL, Lindemann R. Dynamic tensile strength of concrete materials. Supplement to Title 68-8 ACI Journal, January 1971. Detroit: ACI Publication; 1971.
[22] Riedel W. Beton unter Dynamischen Lasten, meso- und makromechanische Modelle und ihre Parameter. PhD thesis, vol. 5. University of the German Armed Forces Munich: Forschungsergebnisse der Kurzzeitdynamik; 2000.

[23] Schuler H, Mayrhofer C, Thoma K. Experimental determination of damage parameter and implementation into a new damage law. Proceedings of the 11th international symposium on interaction of the effects of munitions with structures, Mannheim, Germany; 2003.
[24] Sluys LJ. Wave propagation, localization and dispersion in softening solids. PhD thesis. Delft University of Technology: Delft University Press; 1992.
[26] Zukas JA, editor. High velocity impact dynamics. New York: Wiley; 1990.